

Hydraulic conductivity imaging by induced polarization and hydraulic tomography

Lukas Römhild¹, Gianluca Fiandaca², and Peter Bayer¹

¹Institute of Geosciences and Geography, Martin Luther University Halle-Wittenberg

²Department of Earth Sciences “Ardito Desio”, Università degli Studi di Milano

1 Introduction

Precise knowledge about the distribution of the hydraulic conductivity K within an aquifer is essential for any type of groundwater modeling. However, in many sedimentary environments, small-scale heterogeneities with highly contrasting hydraulic properties are common, so using averaged K -values derived from sparse borehole data can lead to significant miss-predictions. Therefore, more sophisticated tools are required that can image K with a sufficiently high resolution and accuracy.

Among the geophysical methods, induced polarization (IP) is the most promising tool for K -prediction (e.g., Slater, 2007; Binley & Slater, 2020, for review). Since hydraulic rock parameters as well as the IP response are governed by similar pore space properties, petrophysical relations can be derived from laboratory measurements that allow an estimation of K based on the IP parameters. However, these relations may contain a significant amount of uncertainty due to the inherent scatter of the approximative equations as well as the limited applicability of a petrophysical law derived for a specific set of samples to the actual conditions of the field site.

In contrast, many hydraulic methods (based on different types of pumping tests) exist that allow deriving the hydraulic parameters more directly and are therefore less of a subject to uncertainties in K -estimation. Yet, the hydraulic experiments are usually time-consuming and expensive, so that only sparse data sets are feasible to achieve and the ability to image small-scale structures is limited. Among this group of methods, hydraulic tomography (HT) has become a commonly used tool, which is based on a tomographic cross-borehole setup of pumping tests, similar to seismic cross-well tomography (Yeh & Liu, 2000).

We have implemented inversion procedures for both cross-borehole IP and HT data that allow the direct computation of the K -distribution within unconsolidated, fully saturated sediments. The approaches are tested on a simple synthetic model as well as an aquifer analog data set by performing synthetic IP and HT experiments, contaminating the data with Gaussian noise, and subsequently inverting them for K . We compare the results of the two methods for both test cases and draw conclusions about their advantages and limitations.

2 Induced Polarization

The synthetic IP experiments as well as the IP- K inversion are implemented using EEMverter (Fiandaca et al., 2023), which is an inversion framework for a wide range of geoelectrical and electromagnetic methods. Since our approach is based on time-domain IP, the data space comprises the DC data and the IP decay curves for each quadrupole sequence. The inverse problem is solved based on an iterative Gauss-Newton scheme, where the full-decay IP forward response is computed according to Fiandaca et al. (2012) and Fiandaca et al. (2013). We use a re-parameterization of the classical Cole-Cole model space (Fiandaca et al., 2018) by including two different petrophysical approaches that relate the IP parameters to K : (i) a relation found by Weller et al. (2015) based on the formation factor F and the imaginary part of electrical conductivity σ''

$$k = \frac{\alpha}{F^\beta (\sigma''(1 \text{ Hz}))^\gamma} \quad (1)$$

with the empirical parameters $\alpha = 1.08 \cdot 10^{-13}$, $\beta = 1.12$ and $\gamma = 2.27$, and (ii) an approach based on the relaxation time τ_σ and the diffusion coefficient of the Stern layer D_+ developed by Revil et al. (2012)

$$k = \frac{\tau_\sigma D_+}{4F}. \quad (2)$$

Finally, the conversion from permeability k to hydraulic conductivity K is achieved by

$$K = \frac{d \cdot g}{\eta} \cdot k \approx 7.5 \cdot 10^6 \cdot k, \quad (3)$$

where d is the density of the pore fluid, g the gravitational acceleration and η the dynamic viscosity of the pore fluid. As a result, the model space of the inversion consists of the total DC conductivity σ_0 , the hydraulic conductivity K , the diffusion coefficient D_+ , and the Cole-Cole frequency exponent c . The inversion approach has already been applied to field data, and the K -estimates are mostly comparable with those derived from grain size analysis, slug tests, or direct measurements on borehole samples (Martin et al., 2021; Thalund-Hansen et al., 2023).

3 Hydraulic Tomography

The HT experiments are simulated by using the finite element solver of pyGIMLi (Rücker et al., 2017), where the governing partial differential equation

$$S_s \frac{\partial h}{\partial t} - \nabla \cdot (K \nabla h) = 0 \quad (4)$$

can be implemented, with S_s being the specific storage, K the hydraulic conductivity, and h the hydraulic head. The injection at the pumping locations is simulated as a Neumann boundary condition applied to the respective intervals. Pumping experiments using a Heaviside source are conducted in different depths from top to bottom and the hydraulic head at the different observation intervals in the neighboring boreholes is observed, so that the HT data set consists of the pressure response curves for the respective source-receiver combinations.

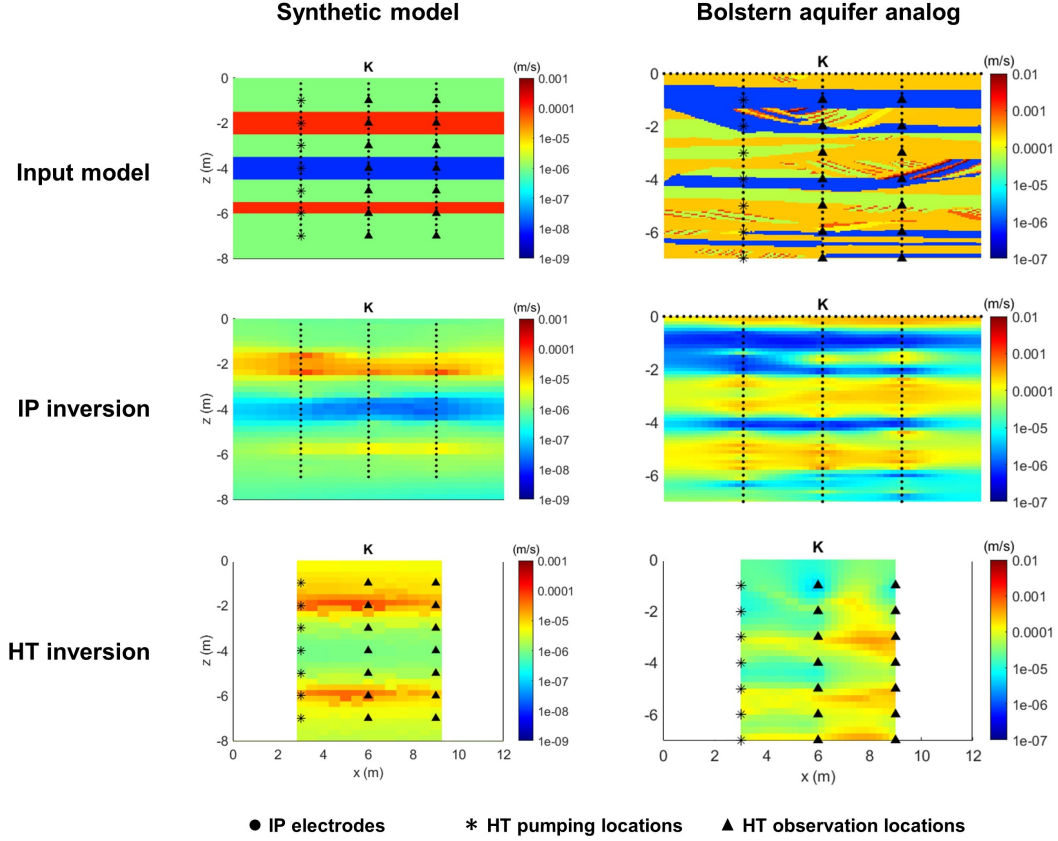


Figure 1: IP and HT inversion results for a purely synthetic model (left part) and the Bolstern aquifer analog data set (right part).

Subsequently, the travel time inversion approach introduced by Brauchler et al. (2003) is applied to the data by picking the travel time of the signal at the maximum of its first derivative and using the 25% early time diagnostics procedure to enhance the sensitivity for the major flow paths. The hydraulic travel time can hence be written as a line integral between the source point x_1 (where the pumping-induced pressure is generated) and the receiver point x_2 (where the hydraulic head is observed), following the ray path ε :

$$\sqrt{t_{\alpha,h}} = \frac{1}{\sqrt{6f_{\alpha,h}}} \int_{x_1}^{x_2} \frac{d\varepsilon}{\sqrt{D(\varepsilon)}}, \quad (5)$$

where $t_{\alpha,h}$ is the early time and $f_{\alpha,h}$ is a conversion factor. Therefore, a standard travel time inversion scheme can be utilized to invert this data set (similar to seismic tomography), derive the distribution of diffusivity D , and ultimately of the hydraulic conductivity K by assuming a constant specific storage S_s .

4 Inversion Results

The two test models as well as the different inversion results are shown in Figure 1. For both cases, three hypothetical boreholes with 3 m distance are implemented, in which the IP electrodes are distributed with 25 cm spacing, and HT source- and receiver-points

with 1 m spacing. Both can be regarded as the smallest feasible spacing for practical applications.

The first synthetic model (left column of plots) consists of different horizontal layers with contrasting hydraulic conductivity. The IP inversion result shows the structural information correctly but has difficulties resolving the strong contrasts between the different layers. In particular, for the thin high- K layer at 6 m depth, K is strongly underestimated, although it may serve as a major flow path within the aquifer. This problem is partly caused by smoothing effects due to regularization, but also a result of the reduced sensitivity of IP to high- K zones, where polarization is typically weak. In contrast, the HT inversion result is particularly successful in reproducing the high- K layers due to the enhanced sensitivity to the major flow paths. However, the low- K layer is not well-defined in the result and the resolution is generally lower due to the larger spacing of source and receiver points compared to IP. Also note that the sensitivity of HT is restricted to the area between the boreholes.

For the second model (right column of plots), data from the Bolstern aquifer analog (Heinz et al., 2003) were used, that are characterized by an alternation of sandy and clayey layers, producing strong contrasts in hydraulic conductivity. Note that in this case, a surface profile was added to the IP electrode sequence. Similar to the first model, the IP results show the structural features correctly and with high resolution, while the K -estimates are particularly precise for the less permeable areas. The HT inversion result still shows the major flow paths of the aquifer correctly, but the ability to retrieve the small-scale structural information is limited. More details about the results for this model can be found in Römhild et al. (2022).

5 Conclusions and Outlook

We have shown that both IP and HT experiments can be used for imaging the distribution of hydraulic conductivity K , when appropriate inversion procedures are applied to the data. By implementing synthetic experiments for two different models, the complementary abilities of the methods can be illustrated:

- (i) While IP has the highest sensitivity to areas of low K due to typically stronger polarization effects, HT is most sensitive to the major flow paths, and thus to areas of high K .
- (ii) Since the HT pumping experiments are typically time-consuming, only a limited number of them is feasible in practice, so that structural information can be retrieved with lower resolution compared to IP, where smaller electrode spacings are commonly used in the field.
- (iii) The K -estimates derived from IP might include significant uncertainties due to bias and scatter by the petrophysical relations, while HT experiments test for the hydraulic parameters directly.

Consequently, the best results can be expected when both methods are employed at the same site, so that the data sets can be used simultaneously. In particular, the structural features of the subsurface may be retrieved by high-resolution IP experiments, while the reliability of the K -estimates is ensured by hydraulic tests (Römhild et al., 2022). Eventually, a joint inversion procedure for both data types could be a promising tool for retrieving highly accurate information about the K -heterogeneities within an aquifer.

References

- Binley, A., & Slater, L. D. (2020). *Resistivity and induced polarization - theory and applications to the near-surface earth*. Cambridge University Press.
- Brauchler, R., Liedl, R., & Dietrich, P. (2003). A travel time based hydraulic tomographic approach. *Water Resources Research*, 39(12), 1370.
- Fiandaca, G., Auken, E., Christiansen, A. V., & Gazoty, A. (2012). Time-domain-induced polarization: Full-decay forward modeling and 1d lateral constrained inversion of cole-cole parameters. *Geophysics*, 77(3), 213-225.
- Fiandaca, G., Madsen, L. M., & Maurya, P. K. (2018). Re-parameterisations of the cole-cole model for improved spectral inversion of induced polarization data. *Near Surface Geophysics*, 16, 385-399.
- Fiandaca, G., Ramm, J., Binley, A., Gazoty, A., Christiansen, A. V., & Auken, E. (2013). Resolving spectral information from time domain induced polarization data through 2-d inversion. *Geophysical Journal International*, 192, 631-646.
- Fiandaca, G., Zhang, B., Chen, J., Signora, A., Dauti, F., Galli, S., et al. (2023). Closing the gap between galvanic and inductive methods: Eemverter, a new 1d/2d/3d inversion tool for electric and electromagnetic data with focus on induced polarisation [Conference Proceedings]. *AEM 2023: Short abstracts*, 52-66.
- Heinz, J., Kleineidam, S., Teutsch, G., & Aigner, T. (2003). Heterogeneity patterns of quaternary glaciofluvial gravel bodies (sw-germany): application to hydrogeology. *Sedimentary Geology*, 158, 1-23.
- Martin, T., Pauw, P. S., Karoulis, M., Mendoza, A., Günther, T., Madsen, L. M., et al. (2021). Inversion of hydraulic conductivity from induced polarisation, part b: Field examples from five countries [Conference Proceedings]. *NSG2021 1st Conference on Hydrogeophysics*.
- Rücker, C., Günther, T., & Wagner, F. M. (2017). pygimli: An open-source library for modelling and inversion in geophysics. *Computers and Geosciences*, 109, 106-123.
- Revil, A., Koch, K., & Holliger, K. (2012). Is it the grain size or the characteristic pore size that controls the induced polarization relaxation time of clean sands and sandstones? *Water Resources Research*, 48.
- Römhild, L., Fiandaca, G., Hu, L., Meyer, L., & Bayer, P. (2022). Imaging hydraulic conductivity in near-surface aquifers by complementing cross-borehole induced polarization with hydraulic experiments. *Advances in Water Resources*, 170, 104322.
- Slater, L. (2007). Near surface electrical characterization of hydraulic conductivity: From petrophysical properties to aquifer geometries - a review. *Surv Geophys*, 28, 169-197.
- Thalund-Hansen, R., Troldborg, M., Levy, L., Christiansen, A. V., Bording, T. S., & Bjerg, P. L. (2023). Assessing contaminant mass discharge uncertainty with application of hydraulic conductivities derived from geoelectrical cross-borehole induced polarization and other methods. *Water Resources Research*, 59, WR034360.
- Weller, A., Slater, L., Binley, A., Nordsiek, S., & Xu, S. (2015). Permeability prediction based on induced polarization: Insights from measurements on sandstone and unconsolidated samples spanning a wide permeability range. *Geophysics*, 80(2), D161-D173.
- Yeh, J., & Liu, S. (2000). Hydraulic tomography: Development of a new aquifer test method. *Water Resources Research*, 36(8), 2095-2105.